ACS NANO

www.acsnano.org

ARTICLE

How the Toughest Inorganic Fullerene Cages Absorb Shockwave Pressures in a Protective Nanocomposite: Experimental Evidence from Two *In Situ* Investigations

Fang Xu,[†,‡] Takamichi Kobayashi,[§] Zhuxian Yang,[†] Toshimori Sekine,[∥,⊥] Hong Chang,[†] Nannan Wang,[†] Yongde Xia,[†] and Yanqiu Zhu*[,†]

[†]CEMPS, University of Exeter, Exeter EX4 4QF, United Kingdom

[‡]Faculty of Engineering, The University of Nottingham, Nottingham NG7 2RD, United Kingdom

[§]National Institute for Materials Science, Tsukuba, Ibaraki 305-0044, Japan

[∥]Department of Earth and Planetary Systems Science, Hiroshima University, Higashi-Hiroshima 739-8526, Japan

[⊥]Centre for High Pressure Science and Technology Advanced Research, Shanghai 201203, People's Republic of China

Supporting Information

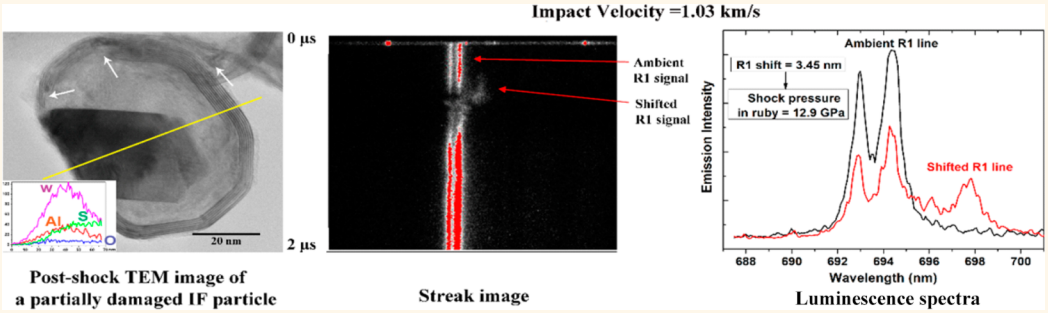

ABSTRACT: **Nanocomposites fabricated using the toughest caged inorganic fullerene WS_2 (IF-WS_2) nanoparticles could offer ultimate protection *via* absorbing shockwaves; however, if the IF-WS_2 nanomaterials really work, how they behave and what they experience within the nanocomposites at the right moment of impact have never been investigated effectively, due to the limitations of existing investigation techniques that are unable to elucidate the true characteristics of high-speed impacts in composites. We first fabricated Al matrix model nanocomposites and then unlocked the exact roles of IF-WS_2 in it at the exact moment of impact, at a time resolution that has never been attempted before, using two *in situ* techniques. We find that the presence of IF-WS_2 reduced the impact velocity by over 100 m/s and in pressure by at least 2 GPa against those Al and hexagonal WS_2 platelet composites at an impact speed of 1000 m/s. The IF-WS_2 composites achieved an intriguing inelastic impact and outperformed other reference composites, all originating from the "balloon effect" by absorbing the shockwave pressures. This study not only provides fundamental understanding for the dynamic performance of composites but also benefits the development of protective nanocomposite engineering.**

KEYWORDS: *shock absorbing, impact velocity, inorganic fullerene, nanocomposite, shockwave*

Driven by the practical needs, the development of advanced shock-absorbing composites based on nanomaterials has been proposed for over a decade.[1] Nanocomposites, either being stronger and/or more absorbing than their single-phased counterparts, are highly desirable for next generation protective armory applications.[1] In particular, as the toughest cage structures, individual inorganic fullerene WS_2 (IF-WS_2) and IF-MoS_2 nanoparticles are superb shock absorbers and can survive shockwave pressures up to 25 GPa,[2,3] whereas nanotubes can withstand 21 GPa shockwaves[4] and exhibit tensile strengths above 16 GPa.[5] Incorporated into a matrix, such composites have been predicted to be a few times better than the best impact resistant materials (*e.g.*, SiC, B_4C) used in protective armor,[6] which will boost their applications well beyond the proven excellent electronic and tribological properties.[5,7−13] Hence, the structures and extraordinary shock-

Received: April 28, 2017
Accepted: August 4, 2017
Published: August 4, 2017

DOI: 10.1021/acsnano.7b02943
ACS Nano 2017, 11, 8114−8121

absorbing properties of these IFs have been associated with an emerging class of energy-absorbing protective nanocomposites—named "NanoArmour",[6] but this hypothesis highlighted by Hogg in Science[1] has yet to be validated experimentally.

Precisely evaluating the shock/ballistic characteristics and gaining fundamental understanding toward the performance of complex composite systems are extremely challenging because of the difficulty to carry out real-time investigations at high-speed impact. The recent significantly advanced high-speed digital video cameras in combination with computer simulations are probably the best techniques to date;[14,15] however, the resolution at the macroscopic level restricts it from revealing the real-time shock behavior of nanocomposites at the super short moment with details, which also makes the simulations hard to be validated at the nanoscale.

IF-WS_2 nanoparticles have been incorporated with a wide range of polymer matrices previously,[16,17] and they have effectively improved thermal, mechanical, and tribological properties, even the toughness of the composites;[17] however, there were hardly any reports focusing on other matrices reinforced by these IF nanoparticles. Here, we report two very innovative and specialized *in situ* impact techniques in geophysics: the time-resolved luminescence[18,19] and the velocity interferometer system for any reflector (VISAR) techniques,[20,21] combined with postshock analyses, to investigate the impact performance of such IF-WS_2 containing Al model nanocomposites and to scrutinize their precise roles in impacts, by contrasting with the conventional bulk 2H-WS_2 (the hexagonal WS_2 platelets) composites.

RESULTS AND DISCUSSION

The as-produced IF-WS_2 particles were around 30−80 nm in size (mostly 40 nm), exhibiting a typically multilayered close-caged structural feature (Figure 1a).[22] We used a hot-press to

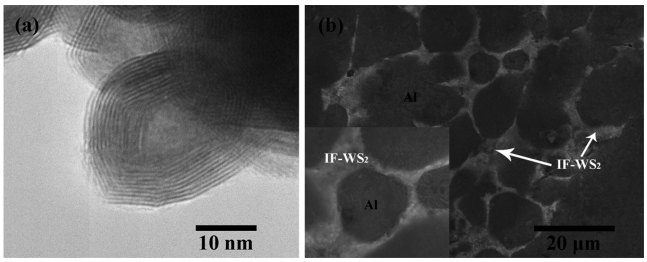

Figure 1. TEM image of the as-produced IF-WS_2 nanoparticles (a) and SEM image of the 30 wt % IF-WS_2-reinforced Al composites (b). The as-produced IF-WS_2 particles are around 30−80 nm in size (mostly 40 nm), with *ca.* 15 seamless layers and a layer separation of 0.62 nm (a). IF-WS_2 nanoparticles are fairly uniformly distributed in the Al matrix, between the Al grain boundaries, and the average size is ∼20 μm (b). The tiny white dots in the inset show the IF-WS_2 nanoparticles.

create the IF-WS_2-reinforced Al model nanocomposites for this research, whereas pure Al and 2H-WS_2-reinforced Al nanocomposites were also produced as referenced counterparts, following the same process. After being polished and slightly etched, the particle distributions in the Al matrix were clearly shown under scanning electron miscroscopy (SEM). The IF-WS_2 (white phases) were fairly uniformly distributed along the grain boundaries among the larger Al grains (dark phases) (Figure 1b), given the process limitation of powder metallurgy and such a high loading in the matrix. In general, the matrix Al grains in the IF-WS_2 composites were slightly smaller than thoe of the 2H-WS_2 composites and pure Al (Table S1 in Supporting Information, SI). This showed directly the grain size reduction effect of the fillers in composites and was also an indirect indication of the good distribution of the fillers within the matrix, as a poor filler distribution would lead to dramatically irregular grain sizes of the matrix.

The VISAR experiments measure the particle velocities during impact,[20,23−26] and the detailed setup is described in Figure S1 (SI). A summary for each sample description and experimental parametres are also listed in Tables S1 and S2 in the SI.

We performed three series shots of VISAR measurements at impact velocities of 1.43 ± 0.03, 1.735 ± 0.025, and 1.062 ± 0.027 km/s, as shown in Figure 2a−c, respectively, to evaluate the different impact speed responses of the composites. In general, the window/sample interface particle velocity profiles displayed a sharp increase corresponding to the shockwave arrival, plateau for 0.7−0.8 μs, then followed by a decrease for 0.5−0.6 μs, and a second plateau at nearly half velocity of the first plateau except for samples B3 and C3. The measurements at ∼1 km/s were successful only for a short period of ∼1.2 μs. Using the window shock data (fused quartz),[27] the pressure at the plateau is calculated to be ∼13.4 and ∼6.8 GPa in Figure 2a, ∼17.4 and ∼9.2 GPa in Figure 2b, and ∼10.3 and ∼4−5 GPa in Figure 2c. The initial shock pressure for the sample was slightly higher than the calculated value due to the impedance mismatch between the sample and the window. When the projectile traveled at a speed of 1.4 km/s, there were barely any differences among the samples (Figure 2a). Similarly, the performance of samples being struck at the initial velocity of 1.735 km/s largely resembled those of 1.4 km/s, with minor differences (Figure 2b). The tested samples displayed no distinct differences between impact speeds of 1.43 and 1.735 km/s, and all the resulting velocities were quite stable, except sample D appeared to have lower velocities after shock (Figure 2a,b).

However, when the projectile traveled at a speed of around 1 km/s, the samples behaved differently. Samples A, B, and C were still quite similar, but samples D and E (containing IF-WS_2 nanoparticles) exhibited vastly different features (Figure 2c). The velocity signals started to appear at around 2.8 μs, with starting values of about 0.8 km/s for samples D and E, but around 0.9 km/s for samples A, B, and C, that is, a 0.1 km/s (100 m/s) difference. Significantly, an immediate increase in velocities for samples A, B, and C was observed at the time of 3 μs, which peaked at 1 km/s for sample B and at 0.95 km/s for sample A, compared to only 0.85 km/s for samples D and E. Following these sudden surges, the velocities underwent an unstable period (3.1−3.4 μs) and were seen to drop slowly, in contrast to the very steep slopes observed for samples being shocked at 1.43 and 1.735 km/s, although both also demonstrated a significant decay of about 60% in the second state of shot, which is indicative of absorption of shock energy. Because of these significantly different features that were exhibited at the low impact speed region, our second *in situ* investigations were focused on the 1 km/s velocity.

The time-resolved luminescence experiments recorded the streak image of ruby luminescence when the shockwaves struck the test samples and the ruby window (Figure S2 in SI), and the results are shown in Figure 3 at impact velocities of ∼1.0 km/s.

DOI: 10.1021/acsnano.7b02943
ACS Nano 2017, 11, 8114−8121

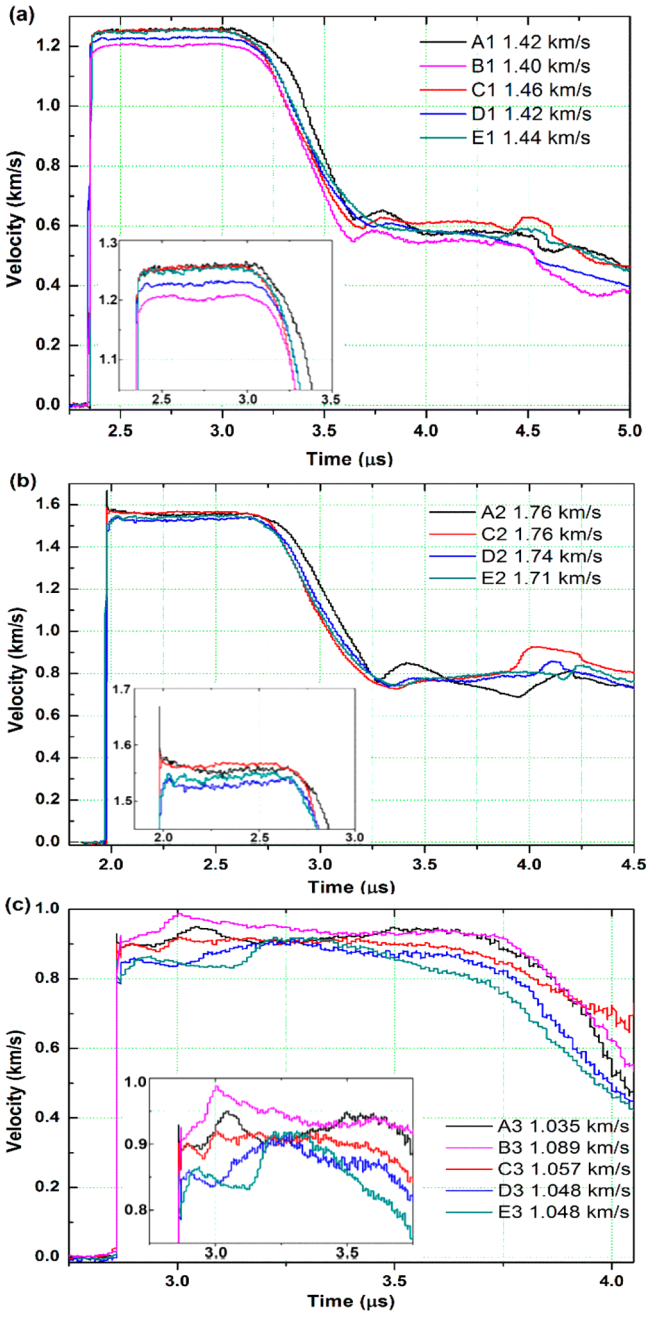

Figure 2. Window/sample interface particle velocity profiles for SiO_2 window and composites samples (A, pure Al; B, 20 wt % 2H-WS_2-reinforced Al composites; C, 30 wt % 2H-WS_2-reinforced Al composites; D, 20 wt % IF-WS_2-reinforced Al composites; E, 30 wt % IF-WS_2-reinforced Al composites). The impactors were accelerated by a propellant gun and struck the base plate (where the test samples were attached) at three speeds of 1.43 ± 0.03 km/s (a), 1.735 ± 0.025 km/s (b), and 1.062 ± 0.027 km/s (c). Inset shows the enlarged profiles for each experiment until the speed dropped. When the projectile traveled at a speed of 1.43 km/s (a), there were barely any differences among the samples, particularly for samples A, C, and E possessing the same velocity and being very stable at about 1.25 km/s in the time window of 2.4−3.1 μs. The tiny differences in the initial impact speeds, sample A (pure Al) being the lowest (1.42 km/s), sample C (Al, 30 wt % 2H-WS_2) the highest (1.46 km/s), and E (Al, 30 wt % IF-WS_2) between (1.44 km/s), led to the lowest velocity reduction after shock for sample A. Similarly, the slightly lower velocities for samples B (Al, 20 wt % 2H-WS_2) and D (Al, 20 wt % IF-WS_2) were also believed to have resulted from the lower starting impact speeds. The performance of samples being struck at the initial velocity of 1.735 km/s exhibited minor differences, though samples D and E showed lower velocities after the shockwave impact (b). The samples behaved very differently when the projectile traveled at a speed of around 1.0 km/s (c).

It is imperative to note that the points at which the shifted R1 and R2 lines appeared (due to the initial impact-induced compression shockwaves), until the original ambient R signals almost completely disappeared, corresponded to the entire period when the shockwaves had just finished traveling through the ruby window and reached the free surface. Then the shockwaves were reflected back into the ruby window, as a release wave, which was represented by the moment the shifted R lines gradually lost their intensity. The original R lines regained the intensity until the release wave reached the sample/ruby interface. The negatively shifted R line signals observed at around 1 μs (Figure 3a,c) were attributed to the interaction of rarefaction from ruby edges.[28] Based on the pressure-shift characteristics of the ruby crystal,[19,29] we can then determine the shock pressures on the ruby, corresponding to each exact stage of the impact compression.

In this work, the pressure was calculated based on the stronger R1 signal. For sample B, the 3.29 nm shift of R1 (Figure 3b) corresponded to a shock pressure of ∼12.4 GPa. This was below the Hugoniot elastic limit (HEL) of ruby, which was 14 GPa, suggesting the ruby window was shock compressed elastically.[19] In addition, the shifted R1 line is very strong, with intensity almost 66% of intensity for the ambient R1 line. Indeed, the strong and sharp shifted R1 line, as well as the negatively shifted R lines, represented the typical elastic region signals.

Similarly, a strong and sharp R1 line shift had also been observed for sample A (Figure S3 in SI) and samples C (Al, 30 wt % 2H-WS_2, Figure 3c,d), as well as the negatively shifted lines, suggesting the typical elastic signals. From the luminescence spectra, we obtained a 3.33 nm shift of the R1 signal for both samples A and C, which corresponded to the shock pressure of 12.5 GPa in ruby, whereas the intensity is 68% compared to that of ambient R1 for sample A and 78% for sample C.

Sample D (Al, 20 wt % IF-WS_2), however, exhibited different features if we compare Figure 3e with Figure 3a: the shifted R lines were very blurred and short, and no negatively shifted lines were observed with only slight yet blurry vibrations of the lines. In Figure 3e, the start of shock compression and the final shockwave release took place within a period of 500 ns (between 0.5 and 1 μs in the time scale), whereas in the case of sample B, it lasted for almost 1000 ns (0.5−1.5 μs). The shorter interval implies a faster release of shocked state in the case of sample D, suggesting that the ruby window and the sample have gone through different structural changes from those cases for samples A, B, and C.

The extracted wavelength profiles of sample D (Figure 3f) showed a 3.45 nm shift for the R1 signal, which corresponded to the shock pressure of 12.9 GPa in ruby. However, the compression-shifted R1 signal for sample D (Figure 3f) was much weaker than that of sample B (Figure 3b), consistent with the more blurred signals in the streak image. Significantly, the intensity of the shifted R1 was much weaker, with only 32%

DOI: 10.1021/acsnano.7b02943
ACS Nano 2017, 11, 8114−8121

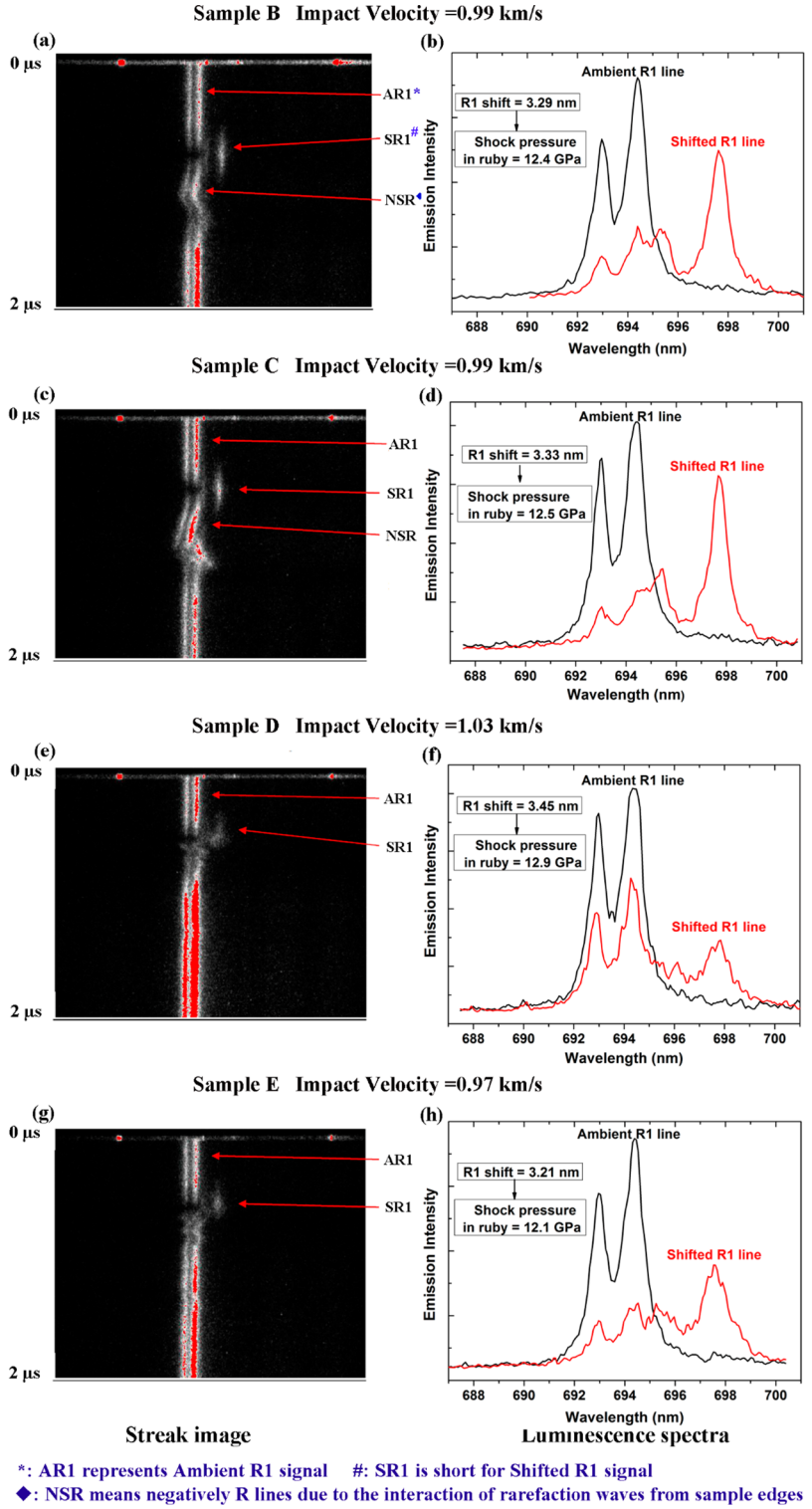

Figure 3. Streak images and luminescence spectra of ruby from sample B (a,b) with 20 wt % 2H-WS_2 reinforcement, sample C (c,d) with 30 wt % 2H-WS_2 filler, sample D (e,f) with 20 wt % IF-WS_2 filler, and sample E (g,h) with 30 wt % IF-WS_2 reinforcement. The vertical axis in the streak image represents the time sequence from top to bottom, with a full scale of 2 μs (a,c,e,f). The two bright parallel vertical lines were the ambient ruby R lines, appearing in the upper and lower part of the image, where the left one was R2 at 692.9 nm (gray) and the right one was R1 at 694.3 nm (highlighted in red). When the ruby crystal was shock compressed, shifted R lines appeared, as shown in the upper part of the image. The ambient R lines then appeared again in their original positions, and negatively shifted R lines were also observed subsequently, followed by another slightly shifted signal and then regained their original intensities and positions, and finally came back to normal ambient R signals. The ruby luminescence spectrum at a chosen instance was obtained by taking the horizontal cross section of the streak image at a time frame of ~0.1 μs (b,d,f,h). The ruby luminescence wavelength recorded in the horizontal axis increased from left to right, with a full width range of 15 nm for the chosen instance.

DOI: 10.1021/acsnano.7b02943
ACS Nano 2017, 11, 8114–8121

Table 1. Summary of the Main Features of *In Situ* Luminescence Streak Images and Spectra from Different Samples[a]

	A	B	C	D	E
R1 shift	3.33 nm	3.29 nm	3.33 nm	3.45 nm	3.21 nm
corresponding pressure	12.5 GPa	12.4 GPa	12.5 GPa	12.9 GPa	12.1 GPa
feature of shifted R1	strong and sharp, negatively shifted	strong and sharp, negatively shifted	strong and sharp, negatively shifted	blurry/weak and short, no negative shift	blurry/weak and short, no negative shift
shifted R1 intensity/ambient R1 intensity	78%	66%	68%	32%	46%

[a]A: pure Al. B: 20 wt % 2H-WS_2-reinforced Al composites. C: 30 wt % 2H-WS_2-reinforced Al composites. D: 20 wt % IF-WS_2-reinforced Al composites. E: 30 wt % IF-WS_2-reinforced Al composites.

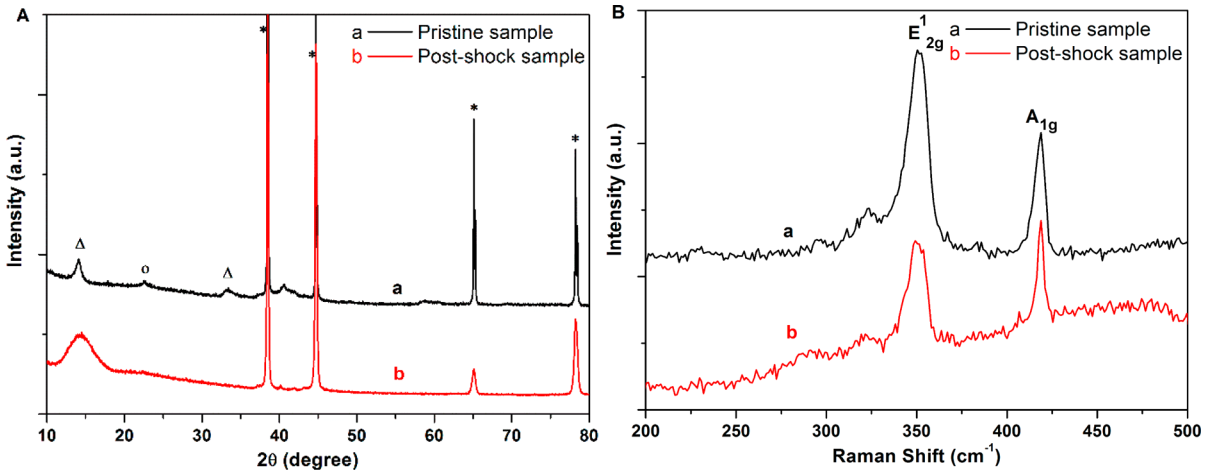

Figure 4. XRD patterns (A) and Raman spectra (B) of the before (a) and postshock (b) samples (sample D: 20 wt % IF-WS_2-reinforced Al composites). In the XRD patterns (A), peaks labeled with a star were matched with the Al phase, and the peaks labeled with a triangle were assigned to the IF-WS_2 and 2H-WS_2 phases; the residual WO_x phases were represented by the circle labeled peak.

intensity compared to that at ambient pressure (Figure 3d), and the very weak, broad, and short characteristics of such shifted R lines were indicative of an inelastic region signal.[19] This is very surprising, as the shock pressure was below the HEL of ruby.

Sample E (Al, 30 wt % IF-WS_2) shock compressed at an impact velocity of 0.97 km/s also exhibited a streak image and luminescence spectra (Figure 3g,h) similar to that of sample D, with weak and blur shifted signals and without negative shift. The shift of R1 signal was 3.21 nm, corresponding to a shock pressure of 12.1 GPa in ruby. The intensity of shift R1 is only 46% of that of ambient R1, close to 32% in sample D, indicating an inelastic region signal.

From the luminescence results, we can distinguish the two different types of behavior for our samples (Figure 3 and Table 1): samples A, B, and C exhibiting a stronger and sharper shifted R1 line accompanied by a negative shift, signifying the typical elastic region signal; samples D and E (containing IF-WS_2) having similarly very weak, broad, and short shifted R1 signal, evidencing the inelastic region characteristics.[19] These results have confirmed that for samples D and E, the ruby crystal windows responded inelastically in the elastic region below the HEL of ruby. Further, this suggests that the shockwave propagation characteristics in samples D or E were somehow changed, from a normal plane shockwave to nonplanar. It is interesting to find out that the target composite samples D and E have shown the inelastic responses at low shock pressures, as much as >2 GPa lower than the elastic limit.

In ceramics, fracture and dislocation are normally attributed to inelastic deformation, though the mechanism remains to be fully clarified.[30] In this case, by considering the complementary experiments for other composite samples, we believe that the inelastic response of the ruby window should be attributed to the intrinsic features of the IF-WS_2 nanocomposites. This is quite convincing because such phenomena were only observed for samples containing IF-WS_2, despite the different concentrations and densities in the composites, not for pure Al and 2H-WS_2 containing composites. It is likely that the previously proposed shock-absorbing property of the IFs[2−4] in the nanocomposites have changed the original feature of the shockwaves, either through their hollow close-caged structure or working as a balloon/spring when they travel through the samples, resulting in the first set of compression-shifted R signals.

The results from both the VISAR and time-resolved luminescence agreed very well with each other; both confirmed similar performance of samples D and E (IF-WS_2 containing composites) and are different from other samples (either pure Al or 2H-WS_2 containing composites). Compared with the VISAR shots, in the time-resolved luminescence experiment, the pressure corresponding to an impact velocity of 1.0 km/s increases due to the high impedance of ruby. Actually, ruby shots in the luminescence experiment correspond almost to Figure 2a at 1.4 km/s (P = ∼13 GPa). VISAR looks at the interface velocity, but the ruby luminescence looks at the pressure it experiences. However, the behavior of samples D and E containing IF-WS_2 nanoparticles differs from others containing 2H-WS_2, as shown by both VISAR shots and ruby time-resolved luminescence experiments. When the samples were struck by shockwaves with impact velocity of around 1.00 km/s, we have found that this type of IF-WS_2 containing composites had lower particle velocities under shock impacts

DOI: 10.1021/acsnano.7b02943
ACS Nano 2017, 11, 8114−8121

and exhibited an unexpected inelastic signal at the elastic region of ruby.

The immediate question is why and how the IF-WS_2 caused the above differences in the composites. To answer this question, we have managed to recover sample D after the VISAR test and conducted postshock analyses in an effort to understand what exactly happened to the composites during the shock, to unlock the secret roles of the IFs in the composites, and to reveal the reinforcing mechanism.

Compared with the X-ray diffraction (XRD) results of the original composite samples (for details, see Figure S4 in SI), the IF-WS_2 peaks of the postshock sample were quite similar to the preshock samples (Figure 4A), and only the (002) peak was broadened and slightly shifted to higher angle, with higher relative intensity.[31,32] These composite samples also exhibited similar Raman features, and the Raman peaks at 349 and 419 cm^{-1} (Figure 4B) were assigned to the $1E_{2g}$ and A_{1g} modes of IF-WS_2,[32] respectively. The slight broadening of the $^1E_{2g}$ peak and sharpening of A_{1g} were observed in the postshock sample, which could be related with the increased nanometer-sized 2H-WS_2 content in the specimens due to shock damage/breakage.[3,33,34]

Figure 5a shows the transmission electron microscopy (TEM) image of an isolated IF-WS_2 nanoparticle in the Al matrix (*ca.* 70 nm in size), prior to impact tests. The morphologies of the IF-WS_2 in the as-prepared composites exhibited no difference from the loose IF-WS_2 nanoparticles (Figure 1a), though smaller particles (<40 nm) started to exhibit smooth olive-shaped structure and larger particles (>40 nm) adopted a rigid polyhedral shape. This shape difference could affect their performance under shockwaves, as stated in our previous work.[3]

After being recovered from a high-impact velocity of 1.74 km/s, damages of different extents have been observed, and several different particles are shown in Figure 5b (1.74 km/s), where the particles were still attached to a large piece of Al matrix whose surface appeared to be cracked. There were also unusal solid dark phases that did not exist in the pristine IF-WS_2, and it is most likely that they were the evidence left behind from the shockwave impact. Indeed, considering the planar shockwave propagation during impact, we knew that the shockwaves traveled along one direction within the composites. Therefore, based on the trajectory subjected to a similar impact direction, it was shown that the dark phases were postshock insertions (Figure 5b). Smaller intact particles observed on the top of these two broken larger IFs showed that smaller IF particles were indeed capable of sustaining higher shock pressures than larger particles even surrounded by a matrix in the composites. It is in good agreement with our previous studies based on loose particles and confirmed the implication that the smaller the IF size the better the shock-absorbing property.[2] This fact that smaller particles correspond to less extent of damage has also suggested that the shock-absorbing properties of the composites could have been improved if all the IF particles were of uniform and smaller size.

Figure 5c (1.74 km/s) showed clearly a third body part insertion from the left into the hollow core of the IF-WS_2 particle (verified by rotation of the sample), and the dark insertion was confirmed to be loose Al grain by using an energy-dispersive X-ray spectroscopy line scan across the particles (bottom left inset in Figure 5c). Severe damages to the top particles were visible, as indicated by the arrows, though the bottom part survived the impact and appeared intact, with

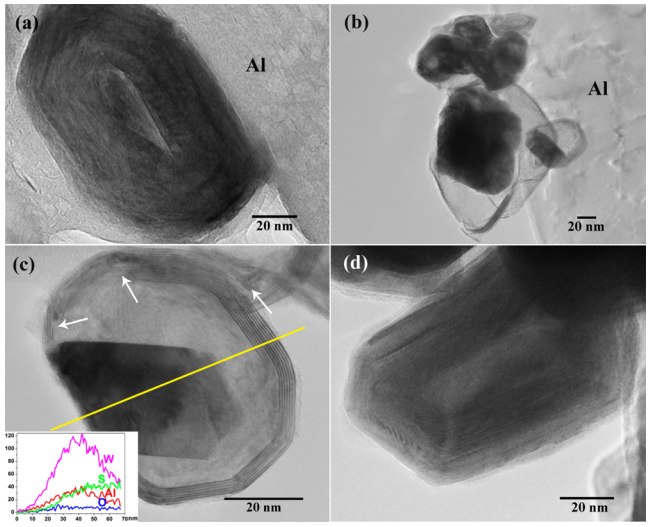

Figure 5. TEM images for postshock samples (20 wt % IF-reinforced Al composites: (a) as-prepared nanocomposites prior to impact test, (b,c) recovered from sample D2 subjected to impact velocity of 1.74 km/s, and (d) recovered from sample D3 after shockwave at 1.048 km/s. Isolated IF-WS_2 nanoparticle in the Al matrix (*ca.* 70 nm in size), prior to impact tests, is demonstrated in (a), exhibiting a multilayered completed close-caged structural feature, resembling that of as-produced IF-WS_2. Several different particles were shown in (b); the particles were still attached to a large piece of the Al matrix whose surface appeared to be cracked, due to the Ar ion bombardmant during the TEM specimen thinning process. This was a good indication of the interface connection between the IF-WS_2 and the Al matrix grains. In (c), severe damages were visible at the top part of the particle: missing layers from the inner core (the left arrow), partially broken and mismatched shells or layers (the middle arrow), and peeled off layers (the top right arrow). However, the bottom part survived the impact and appeared intact, demonstrating features similar to those of the pristine IFs. Nearly intact IF-WS_2 particles were observed (d) as the dominant feature in the specimen subjected to lower shock velocity (1.04 km/s).

perfect WS_2 lattice fringe and smooth corners, akin to the pristine IFs. Nearly intact IF-WS_2 particles subjected to lower shock velocity (1.04 km/s) were observed as the dominant feature in the specimen, and the olive-shaped structure was well-preserved in postshock composites, as shown in Figure 5d.

The postshock characterizations, particularly the high-resolution TEM images, have revealed the shockwave-induced breakages/damages of the larger IF-WS_2 particles. As discussed earlier, during the shockwave propagation through the nanocomposites, the breakage or collapse of IFs must also have absorbed the impact pressure in a way similar to other dense and conventional solid materials. In this regard, the stronger and the tougher the materials, the better the performance for the materials to stop penetration during impact. The IF-WS_2 and the 2H-WS_2 resulted in similar densities, filler distribution, hardness (indeed IF-WS_2 resulted in lower hardness than the 2H-WS_2 in composites), and other static mechanical properties for the composites (Table S1 in SI). Therefore, the dynamic performance differences (*i.e.*, the changes in the pressure profiles and the inelastic behavior of the IF-WS_2 nanocomposites against composites containing the same fractions of 2H-WS_2) pointed to other new directions, and they must be the consequences of the structural differences between IF-WS_2 and 2H-WS_2 reinforcements. The IF-WS_2

DOI: 10.1021/acsnano.7b02943
ACS Nano 2017, 11, 8114–8121

nanoparticles in the composites reduced the particle velocity of the composites and led to the unexpected inelastic response of ruby at least 2 GPa below its HEL pressure of 14 GPa. The response of the ruby is a direct reflection of the performance during the impact; therefore, the inelastic phenomena we reported here have provided convincing evidence for the damping effect of the IF-WS_2, at the exact moment of the impact on the composites.

To understand how this damping effect worked under dynamic shockwaves, we need to consider our recovery results again. First, it seems that the perfectly intact hollow structure of the IFs in the composite could act as molecular-sized voids to absorb the shock pressures, which could lead to the inelastic effect (Figure 5b). Second, the multilayered cages could also act as a "balloon" *via* a spring-like response to absorb the shock pressure.[2] It is understandable that a spring-like effect will generate an accompanying bouncing effect, which should disturb the propagation of plane shockwaves in the IF composites (Figure 2c) but not in other (2H-WS_2) composites. Third, the partially damaged (verified by XRD and Raman in Figure 4) and the third party (Al) insertion into the hollow IF-WS_2 cage, as observed in Figure 5c, could absorb energy and lead to more unstable velocities (Figure 2e) and quicker velocity drops (Figure 3e,f) compared to that of normal 2H-WS_2 composites. During the shockwave propagation within the sample thickness direction, the observed layer peeling off, cage collapse, and Al grain insertion into the cage would have taken place gradually within the entire process, including the bouncing wave propagations, hence leading to unstable particle velocities. Finally, whereas these damages/breakages gradually happened, the damping effect should be taking place concurrently, thus resulting in faster velocity drop than that with either pure Al or 2H-WS_2 composites, which only suffered from conventional deformations and cracks after being subjected to the same shocking process. We believe this indeed was the case for the IF-WS_2 composites, not for 2H-WS_2 or even other nanoparticulate-reinforced nanocomposites.

CONCLUSIONS

To conclude, the present results provide the experimental evidence to show that the IF-WS_2 nanoparticles effectively dampened the peak shock pressure, reduced the measured velocity by about 40% against the calculated velocity for the second state, changed the shockwave propagation at all impact speeds, and led to the unexpected inelastic response in the composites at low impact speed. Based on this real-time information, assisted with postshock analyses of the composites, we have attributed the interesting performance to the intrinsic shock-absorbing properties of IF-WS_2 nanoparticles that originate from their fullerene-like hollow cages. The 100 m/s particle velocity reduction out of 1000 m/s and the over 2 GPa pressure reduction to achieve an inelastic impact can be viewed as directly converted to equivalent reinforcing effects of this class of shock-absorbing composites, beyond the model Al matrix. The methodology used to gain these fundamental understandings about the intriguing roles of IF-WS_2 in composites during the exact moment of impact will significantly boost nanocomposite research and benefit future advanced nanocomposite design and engineering. More effort is required to create high-performance IF-WS_2-reinforced composites to turn the "NanoArmour" science fiction into an engineering reality.

EXPERIMENTAL SECTION

IF-WS_2- and 2H-WS_2-reinforced Al composites were prepared, respectively, by effective ultrasonic mixing and hot-press sintering, as was the pure Al sample. Time-resolved particle velocities at the interface between the sample and fused quartz window were measured by a velocity interferometer, VISAR (VALYN MULTI-BEAM VISAR system), using a single stage propellant gun with a 30 mm inner-bore diameter. Time-resolved luminescence spectroscopy has been applied to record and reveal the pressure shift of the ruby window during the shock impact generated by a propellant gun. SEM, Raman, XRD, and high-resolution TEM were employed to examine the morphology and structure characteristic of both as-prepared and postshock composites, particularly to reveal the structure changes by the shock process. Full methods and any associated references are available in the Supporting Information.

ASSOCIATED CONTENT

Supporting Information

The Supporting Information is available free of charge on the ACS Publications website at DOI: 10.1021/acsnano.7b02943.

Full composite synthesis methods, detailed characterization techniques, additional details on the two *in situ* experiments, extra testing results, and discussion are presented as Figures S1−S4, Tables S1 and S2, including associated references (PDF)

AUTHOR INFORMATION

Corresponding Author

*E-mail: y.zhu@exeter.ac.uk.

ORCID

Yanqiu Zhu: 0000-0003-3659-5643

Notes

The authors declare no competing financial interest.

ACKNOWLEDGMENTS

The authors thank EPSRC for financial support.

REFERENCES

(1) Hogg, P. J. Composites in Armor. *Science* **2006**, *314*, 1100−1101.

(2) Zhu, Y. Q.; Sekine, T.; Li, Y. H.; Wang, W. X.; Fay, M. W.; Edwards, H.; Brown, P. D.; Fleischer, N.; Tenne, R. WS_2 and MoS_2 Inorganic Fullerenes-Super Shock Absorbers at Very High Pressures. *Adv. Mater.* **2005**, *17*, 1500−1503.

(3) Zhu, Y. Q.; Sekine, T.; Li, Y. H.; Fay, M. W.; Zhao, Y. M.; Poa, C. H. P.; Wang, W. X.; Roe, M. J.; Brown, P. D.; Fleischer, N.; Tenne, R. Shock-Absorbing and Failure Mechanisms of WS_2 and MoS_2 Nanoparticles with Fullerene-Like Structures Under Shock Wave Pressure. *J. Am. Chem. Soc.* **2005**, *127*, 16263−16272.

(4) Zhu, Y. Q.; Sekine, T.; Brigatti, K. S.; Firth, S.; Tenne, R.; Rosentsveig, R.; Kroto, H. W.; Walton, D. R. M. Shock-Wave Resistance of WS_2 Nanotubes. *J. Am. Chem. Soc.* **2003**, *125*, 1329−1333.

(5) Kaplan-Ashiri, I.; Tenne, R. Mechanical Properties of WS_2 Nanotubes. *J. Cluster Sci.* **2007**, *18*, 549−563.

(6) Genuth, I.; Yaffe, T. Protecting the Soldiers of Tomorrow; http://www.isracast.com/article.aspx?id=28 (accessed August 10, 2016).

(7) Tenne, R.; Margulis, L.; Genut, M.; Hodes, G. Polyhedral and Cylindrical Structures of Tungsten Disulphide. *Nature* **1992**, *360*, 444−446.

(8) Rapoport, L.; Feldman, Y.; Homyonfer, M.; Cohen, H.; Sloan, J.; Hutchison, J. L.; Tenne, R. Inorganic Fullerene-Like Material as Additives to Lubricants: Structure−Function Relationship. *Wear* **1999**, *225−229*, 975−982.

DOI: 10.1021/acsnano.7b02943
ACS Nano 2017, 11, 8114−8121

(9) Seifert, G.; Terrones, H.; Terrones, M.; Jungnickel, G.; Frauenheim, T. Structure and Electronic Properties of MoS_2 nanotubes. *Phys. Rev. Lett.* **2000**, *85*, 146−149.
(10) Dominko, R.; Arcon, D.; Mrzel, A.; Zorko, A.; Cevc, P.; Venturini, P.; Gaberscek, M.; Remskar, M.; Mihailovic, D. Dichalcogenide Nanotube Electrodes for Li-Ion Batteries. *Adv. Mater.* **2002**, *14* (21), 1531−1534.
(11) Rapoport, L.; Bilik, Y.; Feldman, Y.; Homyonfer, M.; Cohen, S. R.; Tenne, R. Hollow Nanoparticles of WS_2 as Potential Solid-State Lubricants. *Nature* **1997**, *387*, 791−793.
(12) Kaplan-Ashiri, I.; Cohen, S. R.; Gartsman, K.; Ivanovskaya, V.; Heine, T.; Seifert, G.; Wiesel, I.; Wagner, H. D.; Tenne, R. On the Mechanical Behavior of WS_2 Nanotubes Under Axial Tension and Compression. *Proc. Natl. Acad. Sci. U. S. A.* **2006**, *103*, 523−528.
(13) Kaplan-Ashiri, I.; Cohen, S. R.; Gartsman, K.; Rosentsveig, R.; Seifert, G.; Tenne, R. Mechanical Behavior of Individual WS_2 Nanotubes. *J. Mater. Res.* **2004**, *19* (2), 454−459.
(14) Gao, L.; Liang, J. Y.; Li, C. Y.; Wang, L. H. V. Single-shot Compressed Ultrafast Photography at One Hundred Billion Frames Per Second. *Nature* **2014**, *516*, 74−77.
(15) Wen, Y. K.; Xu, C.; Wang, H. S.; Chen, A. J.; Batra, R. C. Impact of Steel Spheres on Ballistic Gelatin at Moderate Velocities. *Int. J. Impact Eng.* **2013**, *62*, 142−151.
(16) Rapoport, L.; Nepomnyashchy, O.; Verdyan, A.; Popovitz-Biro, R.; Volovik, Y.; Ittah, B.; Tenne, R. Polymer Nanocomposites with Fullerene-Like Solid Lubricant. *Adv. Eng. Mater.* **2004**, *6*, 44−48.
(17) Shneider, M.; Dodiuk, H.; Kenig, S.; Tenne, R. The Effect of Tungsten Sulfide Fullerene-Like Nanoparticles on the Toughness of Epoxy Adhesives. *J. Adhes. Sci. Technol.* **2010**, *24*, 1083−1095.
(18) Mao, H. K.; Bell, P. M.; Shaner, J. W.; Steinberg, D. J. Specific Volume Measurements of Cu, Mo, Pd, and Ag and Calibration of the Ruby R1 Fluorescence Pressure Gauge from 0.06 to 1 Mbar. *J. Appl. Phys.* **1978**, *49*, 3276−3283.
(19) Kobayashi, T.; Sekine, T.; Li, X. J.; Yamashita, Y. Observation of Wavelength Shifts in Ruby Under Shock Compression to 36 GPa by Time-Resolved Luminescence Spectroscopy. *Phys. Rev. B: Condens. Matter Mater. Phys.* **2004**, *69*, 054108.
(20) Barker, L. M.; Hollenbach, R. E. Shock-Wave Studies of PMMA, Fused Silica, and Sapphire. *J. Appl. Phys.* **1970**, *41*, 4208−4226.
(21) Barker, L. M.; Hollenbach, R. E. Laser Interferometer for Measuring High Velocities of Any Reflecting Surface. *J. Appl. Phys.* **1972**, *43*, 4669−4675.
(22) Xu, F.; Wang, N. N.; Chang, H.; Xia, Y. D.; Zhu, Y. Q. Continuous Production of IF-WS_2 Nanoparticles by a Rotary Process. *Inorganics* **2014**, *2*, 313−333.
(23) Kobayashi, T. Direct Observation of Large Shock Impedance Jump upon Shock-induced Densification of Powdered Materials Confirmed by *In Situ* Shock Pressure and Particle Velocity Measurements. *Chem. Phys. Lett.* **2014**, *608*, 157−160.
(24) Sekine, T.; Kobayashi, T. Time-resolved Measurement of High-Pressure Phase Transition of Fluorite under Shock Loading. *Phys. Chem. Miner.* **2011**, *38*, 305−310.
(25) Sekine, T.; Kobayashi, T.; Nishio, M.; Takahashi, E. Shock Equation of State of Basalt. *Earth Planets Space* **2008**, *60*, 999−1003.
(26) Kobayashi, T. Particle Velocity Measurements of Powdered Materials under Shock Wave Loading. *Chem. Phys. Lett.* **2015**, *640*, 153−156.
(27) Marsh, S. P. *LASL Shock Hugoniot Data*; University of California: Berkeley, CA, 1980.
(28) Gupta, Y. M.; Horn, P. D.; Burt, J. A. Effect of Tension on R Lines in Ruby Crystals Shocked Along Crystal c Axis. *J. Appl. Phys.* **1994**, *76*, 1784−1788.
(29) Horn, P. D.; Gupta, Y. M. Wavelength Shift of the Ruby Luminescence R Lines Under Shock Compression. *Appl. Phys. Lett.* **1986**, *49*, 856−858.
(30) Grady, D. E. Shock-Wave Compression of Brittle Solids. *Mech. Mater.* **1998**, *29*, 181−203.
(31) Feldman, Y.; Frey, G. L.; Homyonfer, M.; Lyakhovitskaya, V.; Margulis, L.; Cohen, H.; Hodes, G.; Hutchison, J. L.; Tenne, R. Bulk Synthesis of Inorganic Fullerene-Like MS_2 (M = Mo, W) from the Respective Trioxides and the Reaction Mechanism. *J. Am. Chem. Soc.* **1996**, *118*, 5362−5367.
(32) Frey, G. L.; Tenne, R.; Matthews, M. J.; Dresselhaus, M. S.; Dresselhaus, G. Optical Properties of MS_2 (M = Mo, W) Inorganic Fullerenelike and Nanotube Material Optical Absorption and Resonance Raman Measurements. *J. Mater. Res.* **1998**, *13*, 2412−2417.
(33) Joly-Pottuz, L.; Martin, J. M.; Dassenoy, F.; Belin, M.; Montagnac, G.; Reynard, B.; Fleischer, N. Pressure-Induced Exfoliation of Inorganic Fullerene-Like WS_2 Particles in a Hertzian Contact. *J. Appl. Phys.* **2006**, *99*, 023524.
(34) O'Neal, K. R.; Cherian, J. G.; Zak, A.; Tenne, R.; Liu, Z.; Musfeldt, J. L. High Pressure Vibrational Properties of WS_2 Nanotubes. *Nano Lett.* **2016**, *16*, 993−999.

DOI: 10.1021/acsnano.7b02943
ACS Nano 2017, 11, 8114−8121